Probing supersymmetry beyond the reach of LEP2 at the Fermilab Tevatron: Low $|M^3|$ dark matter models

Howard Baer,[1,2,*] Azar Mustafayev,[3,†] Stefano Profumo,[4,‡] and Xerxes Tata[5,§]

[1]*Dept. of Physics, University of Wisconsin, Madison, Wisconsin 53706, USA*
[2]*Dept. of Physics, Florida State University, Tallahassee, Florida 32306, USA*
[3]*Dept. of Physics and Astronomy, University of Kansas, Lawrence, Kansas 66045, USA*
[4]*California Institute of Technology, Mail Code 106-38, Pasadena, California 91125, USA*
[5]*Dept. of Physics and Astronomy, University of Hawaii, Honolulu, Hawaii 96822, USA*

(Received 17 October 2006; published 8 February 2007)

In supersymmetric models where the magnitude of the GUT scale gaugino mass parameter M_3 is suppressed relative to M_1 and M_2, the lightest neutralino can be a mixed higgsino-bino state with a thermal relic abundance in agreement with the WMAP central value for $\Omega_{\rm CDM}h^2$ and consistent with all other phenomenological constraints. In these models, the gluino can be as light as 200 GeV without conflicting with the LEP2 bounds on the chargino mass. Thus, gluino pair production can be accessible at the Fermilab Tevatron at high rates. In this framework, gluinos decay radiatively with a large branching fraction to a gluon plus a neutralino. We find that experiments at the Fermilab Tevatron, with 5 fb^{-1} of integrated luminosity, will be sensitive to $\tilde{g}\,\tilde{g}$ production in the $m_{\tilde{g}} \sim 200$–350 GeV range via the multi-jet + $E_T^{\rm miss}$ and multi-jet + $\ell^+\ell^-$ + $E_T^{\rm miss}$ channels at the 5σ level, while trilepton signatures are expected to be below this level of detectability. Dilepton mass edges from both $\tilde{Z}_2$ and $\tilde{Z}_3$ decays may be measurable in the dilepton + multi-jet + $E_T^{\rm miss}$ channel.

DOI: 10.1103/PhysRevD.75.035004 PACS numbers: 14.80.Ly, 11.30.Pb, 12.60.Jv, 13.85.Rm

I. INTRODUCTION AND MOTIVATION

The determination of the average density of cosmological cold dark matter (CDM) [1]

$$\Omega_{\rm CDM}h^2 = 0.111^{+0.011}_{-0.015}(2\sigma), \tag{1}$$

imposes a stringent constraint on any beyond the standard model framework featuring a weakly interacting massive particle stable on cosmological time-scales.[1] In particular, (1) poses a severe constraint on R-parity conserving supersymmetry (SUSY) models where the lightest neutralino ($\tilde{Z}_1$) is the lightest supersymmetric particle (LSP) [2].

Although it is possible to reconcile the value of $\Omega_{\rm CDM}h^2$ determined by the WMAP team [1] with the thermal neutralino relic abundance $\Omega_{\tilde{Z}_1}h^2$ expected in the framework of the minimal supergravity (mSUGRA) model [3], agreement with (1) is obtained only within narrow regions, most of which are close to the boundary of the allowed parameter space. While the smallness of these regions reflects the impressive precision achieved in the determination of $\Omega_{\rm CDM}h^2$, the fact that they lie close to phenomenologically constrained portions of the parameter space reflects a general result in the mSUGRA setup: except in the case where sparticles are light (the so-called bulk region), $\Omega_{\rm CDM}h^2$ is considerably smaller than the typical mSUGRA expectation for $\Omega_{\tilde{Z}_1}h^2$. Special neutralino annihilation mechanisms can, however, be operative in the Early Universe, enhancing the LSP pair annihilation rate and consequently suppressing its relic abundance to acceptable values. In mSUGRA, instances of such mechanisms are resonant neutralino annihilations through s-channel Higgs exchange diagrams [4], the edges of parameter space where the LSP co-annihilates [5] with either a light stau [6] or a light stop [7], or where $|\mu|$ is small enough so that the LSP features a substantial higgsino component (the hyperbolic branch/focus point (HB/FP) region) [8]. Several groups have examined the signals expected in collider experiments, as well as via direct and indirect searches for neutralino dark matter in underground detectors, assuming that the parameters are in one of these WMAP-allowed regions of the mSUGRA model.

Motivated by the fact that the correlations between the WMAP measurement and expectations in other experiments may be model-dependent, there have been a number of recent studies that have relaxed the universality assumption, that is the hallmark of the mSUGRA framework. Allowing for nonuniversal Higgs boson mass (NUHM) parameters allows for an extended region of parameter space where resonant annihilations occur or/and where $|\mu|$ is sufficiently small [9], while nonuniversality in the $SU(2)$ and $U(1)$ GUT scale gaugino mass parameters allows agreement between $\Omega_{\tilde{Z}_1}h^2$ and $\Omega_{\rm CDM}h^2$ either via an enhanced wino fraction in the LSP [10], or via bino-wino co-annihilation [11]. These extended scenarios can be distinguished from one another, as well as from the mini-

*Electronic address: baer@hep.fsu.edu
†Electronic address: amustaf@ku.edu
‡Electronic address: profumo@caltech.edu
§Electronic address: tata@phys.hawaii.edu

[1]We quote the value obtained by the WMAP collaboration by combining their data with that from the Sloan Digital Sky Survey.

mal mSUGRA scenario, because they give rise to different outcomes for collider signals and for the anticipated detection rates at dark matter search experiments.

Another option to obtain a consistent thermal neutralino relic density is to *reduce* the magnitude of the GUT scale $SU(3)$ gaugino mass M_3 relative to the magnitude of the $SU(2)$ and $U(1)$ gaugino masses [12,13] (the so-called low $|M_3|$ dark matter model (LM3DM)). As explained in Ref. [13], a lowered relic density occurs because a smaller value for $|M_3|$ also induces lower values for the squark masses and the trilinear scalar couplings via the running dictated by the (coupled) renormalization group equations (RGEs). The RGE running also yields a suppression in the absolute size of the soft breaking Higgs mass squared parameter $|m_{H_u}^2|$, which, in turn, lowers the magnitude of the weak scale superpotential mass parameter $|\mu|$ (fixed by the value of M_Z), so that the lightest neutralino develops a significant higgsino component, giving rise to mixed higgsino dark matter (MHDM).[2] Agreement with WMAP is then obtained because the neutralino annihilation rate is enhanced by larger annihilation amplitudes into gauge and Higgs boson pairs, and co-annihilation with the lightest chargino and the next-to-lightest neutralino further suppress the final LSP relic density.

In the LM3DM scenario, we generically expect the ratio of the gluino to lightest chargino mass $m_{\tilde{g}}$:$m_{\tilde{W}_1}$ to be *smaller* than the corresponding value ~3–3.5 expected in models with universal GUT scale gaugino masses and large $|\mu|$. This ratio is important when comparing collider searches for sparticles with LEP and the Fermilab Tevatron. Assuming that $m_{\tilde{W}_1} - m_{\tilde{Z}_1}$ is not too small and that $m_{\tilde{\nu}} \geq 200$ GeV, consistency with LEP2 experiments requires $m_{\tilde{W}_1} > 103.5$ GeV. For models with gaugino mass unification and large $|\mu|$, this bound implies that gluinos must have mass greater than ~300–350 GeV. Such large mass gluinos are difficult to search for at the Tevatron, as their production cross section is rapidly suppressed with increasing masses.

In the LM3DM model, instead, relatively light gluinos (values of the gluino mass as low as $m_{\tilde{g}} \sim 200$ GeV would be consistent with the LEP2 constraints) can be copiously produced in hadronic collisions, and the currently operating Fermilab Tevatron is the obvious facility to search for these new matter states. To-date, experiments at the Tevatron have searched for gluinos in their multijet plus $E_T^{\rm miss}$ data sample, and exclude gluinos lighter than roughly 200 GeV, irrespective of the squark mass, from their analysis of the Run 1 data [15]. Very recently, the D0 collaboration, from an analysis of 310 fb^{-1} of data has obtained a new limit [16] of $m_{\tilde{g}} > 233$ GeV. Unlike the multilepton plus jets plus $E_T^{\rm miss}$ analyses based on cascade decays of gluinos, inclusive $E_T^{\rm miss}$ analyses are largely independent of the details of the spectrum in the electroweak "*-ino*" sector.[3]

Within any framework with unification of gaugino masses, $m_{\tilde{g}} \sim (3\text{–}3.5)m_{\tilde{W}_1}$, and the published limits from CDF and D0 are pre-empted by the LEP limit $m_{\tilde{W}_1} \gtrsim 103$ GeV on the chargino mass. Within the LM3DM scenario, instead, the gluino is relatively light, and the impact of the LEP chargino limit on the Tevatron gluino search is clearly reduced, so that it is possible that data from Tevatron experiments may probe a range of the LM3DM model parameter space not accessible to LEP2, either in the current data sample, or in the data sample expected to be accumulated at the Tevatron before the LHC completes about a year of operation.

In this study we explore the prospects for detection of gluino pair production within the framework of the LM3DM scenario. The remainder of the paper is organized as follows. In Sec. II we discuss the parameter space and sparticle mass spectra expected in the LM3DM model. In Sec. III, we discuss signal rates and backgrounds for gluino pair discovery in the jets + $E_T^{\rm miss}$ channel. In Sec. IV, we show that discovery in the clean trilepton + $E_T^{\rm miss}$ channel is unlikely. In Sec. V, we show that detection in the dilepton plus multijet + $E_T^{\rm miss}$ is a viable possibility, and that the associated $m(\ell^+\ell^-)$ distribution can give the characteristic mass edges indicative of the $m_{\tilde{Z}_2} - m_{\tilde{Z}_1}$, and, possibly, also of the $m_{\tilde{Z}_3} - m_{\tilde{Z}_1}$ mass difference. Finally, we summarize our results in Sec. VI.

II. THE LOW $|M_3|$ DARK MATTER MODEL

The low $|M_3|$ dark matter model differs from mSUGRA only in that the GUT scale gluino mass parameter M_3 needs not be equal to $m_{1/2} = M_1 = M_2$. The parameter space of this model is thus given by,

$$m_0, m_{1/2}, M_3, A_0, \tan\beta, \text{sign}(\mu), \tag{2}$$

where $m_{1/2}$ is taken to be positive without loss of generality, but M_3 can take either sign. For any set of values for the parameters in (2), we can vary $r_3 \equiv M_3/m_{1/2}$ so as to increase the higgsino content of the LSP and to drive the LSP annihilation rate to yield a relic LSP density $\Omega_{\tilde{Z}_1}h^2$ in agreement with [1]. In order to get $|\mu|$ small enough, we must "*slow down*" the RG evolution of $m_{H_u}^2$ from its GUT scale value of m_0^2 to a negative value at the weak scale—remember that $m_{H_u}^2(\text{weak}) \sim -\mu^2$ as long as $\tan\beta$ is not

[2]Although the gluino mass is reduced from its usual value, the gluino—LSP mass splitting is still large so that gluino co-annihilation can be safely neglected in the evaluation of the $\tilde{Z}_1$ relic density [14].

[3]These analyses are not completely independent of chargino and heavier neutralino masses because the transverse momenta of the $\tilde{Z}_1$ LSPs, and hence the $E_T^{\rm miss}$ spectrum, does depend on the cascade decay patterns. Moreover, sometimes a lepton veto is also imposed on the SUSY signal.

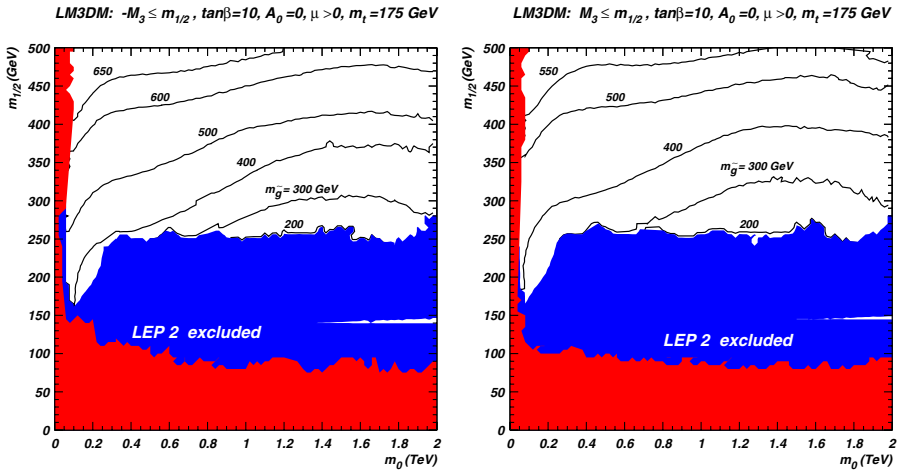

FIG. 1 (color online). Contours of $m_{\tilde{g}}$ in the m_0 vs $m_{1/2}$ plane for the LM3DM model, where $M_3(M_{\rm GUT})$ has been set, at every point of the parameter space, to the value such that $\Omega_{\tilde{Z}_1}h^2 = 0.11$. We take $A_0 = 0$, $\tan\beta = 10$, $m_t = 175$ GeV, and consider $M_3 < 0$ in the left panel and $M_3 > 0$ in the right panel. The gray (red) regions are excluded because either the electroweak symmetry cannot be correctly broken, or because the LSP is charged. The black (blue) shaded regions are excluded by the LEP2 bound on the chargino mass.

very small—which, in turn, requires a smaller value of $X_t \equiv m^2_{Q_3} + m^2_{t_R} + m^2_{H_u} + A^2_t$ than in mSUGRA. Since gauge coupling effects always *increase* squark mass parameters as they evolve from the GUT scale down to the weak scale, and since the large $SU(3)$ gauge coupling contributes dominantly to this increase, smaller values of X_t are obtained by choosing $|M_3(\text{GUT})|$ to be *smaller* than its mSUGRA value of $m_{1/2}$.

We provide a panorama of the LM3DM scenario in Fig. 1, where we show contours of fixed gluino mass in the $m_0 - m_{1/2}$ plane with $\tan\beta = 10$, $A_0 = 0$ and $\mu > 0$, and where at each point in this plane r_3 has been chosen to obtain the central value given in [1] for the LSP relic density. We use Isajet v7.74 for sparticle mass calculations [17]. The gray (red) region is excluded because either electroweak symmetry in not properly broken or the LSP becomes charged or colored. The black (blue) region is excluded by the LEP2 negative search results for charginos. The wiggles in the plot curves reflect numerical issues related to the precision with which we require the neutralino relic abundance to saturate the WMAP central value for the CDM abundance (1), and also any numerical instabilities in the code for the determination of μ as a function of r_3. On the extreme left of the plot where the gluino mass contours dive, the $\tilde{Z}_1$ is dominantly a bino since (due to light sleptons) the r_3 value there need not deviate severely from $\sim$1. As we move to larger values of m_0 at fixed $m_{1/2}$, much smaller values of r_3 are needed for the neutralino relic abundance to match the CDM density in (1), and we step into the MHDM region which, as explained above, also features a small value of $m_{\tilde{g}}$. Indeed we see that for $m_0 \gtrsim 1$ TeV, the gluino could be lighter than even 200 GeV in a region of parameter space unconstrained by the negative results of sparticle searches at LEP2. Finally, we note that there exists a small white allowed band at $m_{1/2} \sim 150$ GeV in both panels. In this region, neutralinos can annihilate through the light Higgs h resonance, and so the relic density is in accord with WMAP without the need to lower $M_3(M_{\rm GUT})$. Since μ is quite large in this band, the chargino mass is just above the limit from LEP2.

As an example of the relation between sparticle masses in this region of parameter space, we show in Fig. 2(a) the value of $m_{\tilde{g}}$, together with the chargino and neutralino masses (the sfermions are too heavy to be accessible at the Tevatron) versus $m_{1/2}$ for the slice of the plane in Fig. 1 at fixed $m_0 = 1500$ GeV. This m_0 value is representative of the range needed for which $|M_3(\text{GUT})|$ has to be significantly reduced from its mSUGRA value in order to obtain agreement with the observed value of $\Omega_{\rm CDM}h^2$. While in mSUGRA one expects the masses $m_{\tilde{g}}$:$m_{\tilde{W}_1}$:$m_{\tilde{Z}_1}$ to be in the ratio $\sim$7:2:1, we find here that with MHDM, the typical ratio is rather $\sim$2.5:1.5:1, so that not only is the $m_{\tilde{g}} - m_{\tilde{W}_1}$ mass gap reduced, but the $m_{\tilde{W}_1} - m_{\tilde{Z}_1}$ mass gap is suppressed as well. Another noteworthy feature is that because of the smallness of $|\mu|$, there is sizable mixing between gauginos and higgsinos resulting in *three* relatively light neutralinos, while the heavy chargino and the heaviest neutralino (which are dominantly winolike) are considerably split from their lighter siblings. While all the masses increase steadily with $m_{1/2}$, for the $M_3 > 0$ curves (solid lines) we see sharp glitches at very low $m_{1/2} \sim 270$ GeV where $m_{\tilde{Z}_1} < M_W$: for $m_{1/2} < 270$ GeV, very low values of r_3 are needed since $\tilde{Z}_1\tilde{Z}_1 \to W^+W^-$ annihi-

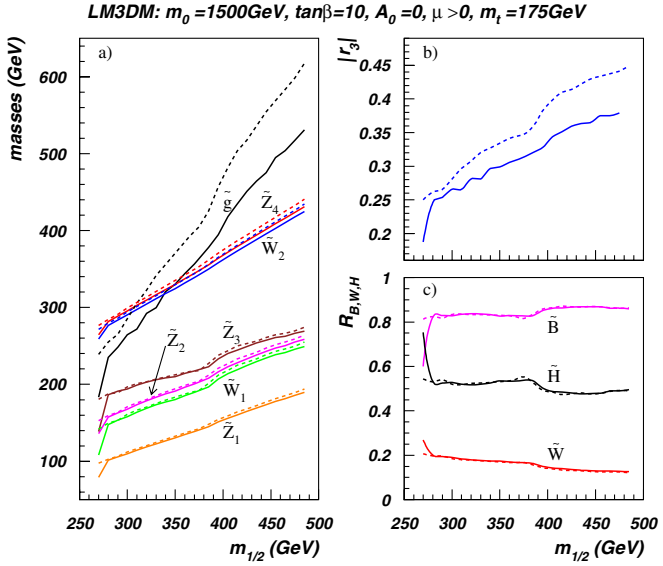

FIG. 2 (color online). In panel (a), we show gluino, chargino and neutralino masses versus $m_{1/2}$ for the LM3DM model where $M_3(M_{\rm GUT})$ has been lowered at every point to obtain $\Omega_{\tilde{Z}_1}h^2 = 0.11$. We take here $A_0 = 0$, $\tan\beta = 10$, $m_t = 175$ GeV and $m_0 = 1500$ GeV. The solid curves correspond to $M_3 > 0$, while the dashed curves to $M_3 < 0$. We cut the curves on the left when the chargino mass falls below its LEP2 bound. In panel (b) we plot the corresponding value of r_3 versus $m_{1/2}$, while in panel (c) we plot the bino/higgsino/wino composition of the $\tilde{Z}_1$ versus $m_{1/2}$.

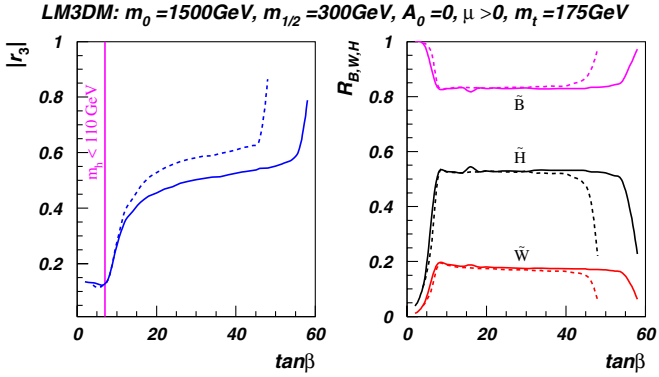

FIG. 3 (color online). In panel (a), we plot $|r_3|$ versus $\tan\beta$ for $m_0 = 1500$ GeV, $m_{1/2} = 300$ GeV, $A_0 = 0$, $\tan\beta = 10$, $m_t = 175$ GeV and $\mu < 0$ (dashed), $\mu > 0$ (solid). In panel (b) we plot the bino/higgsino/wino composition of the $\tilde{Z}_1$ versus $\tan\beta$.

lation in the early universe becomes kinematically suppressed. There are similar glitches for negative M_3 (dashed lines), but these occur for $m_{1/2}$ values excluded by the LEP2 constraints, and are not seen in the figure because we terminate the curves on the left when the chargino mass falls below its LEP2 limit. There is also a slight glitch around $m_{1/2} \sim 380$ GeV, due to turn on of the $\tilde{Z}_1\tilde{Z}_1 \to t\bar{t}$ annihilation mode. We show in panel (b) the corresponding value of r_3 needed to achieve the WMAP-measured relic density: it varies from ~0.2–0.4 over the range of $m_{1/2}$ shown. Finally, in panel (c) we show the bino/higgsino/wino content of the $\tilde{Z}_1$, defined as $R_B \equiv |v_4^{(1)}|$, $R_H \equiv \sqrt{v_1^{(1)2} + v_2^{(2)2}}$ and $R_W \equiv |v_3^{(1)}|$ (the $v_i^{(1)}$ are the higgino, bino and wino components of $\tilde{Z}_1$ in the notation of Ref. [18]), versus $m_{1/2}$: here, it is illustrated that the neutralino is indeed mixed bino/higgsino/wino dark matter over the range of $m_{1/2}$ shown.

In Fig. 3(a), we plot the value of $|r_3|$ versus $\tan\beta$ for fixed values of m_0 and $m_{1/2}$ listed in the figure. For low values of $\tan\beta$, the top Yukawa coupling is increased, and the effect of the $f_t^2 X_t^2$ term in the RGE for $m_{H_u}^2$ is enhanced. As a result, $m_{H_u}^2$ tends to be driven to a more negative value so that MHDM can only be obtained only if r_3 is even smaller than for our canonical choice of $\tan\beta = 10$. For the lowest values of $\tan\beta$ in Fig. 3(a), $m_{\tilde{g}}$ gets close to $m_{\tilde{Z}_1}$ so that neutralino-gluino co-annihilation effects are responsible for achieving the WMAP CDM density.[4] As $\tan\beta$ increases beyond about 10, the value of $|r_3|$ needed to achieve $\Omega_{\tilde{Z}_1}h^2 \sim 0.11$ increases slowly because it becomes increasingly easy to annihilate away the neutralinos (due to large b and τ Yukawa couplings, and lowered third generation sfermion and Higgs boson masses). Near $\tan\beta \sim$ 50–60, the $\tilde{Z}_1\tilde{Z}_1$ annihilation through the A-funnel becomes dominant, and a reduction in $M_3(M_{\rm GUT})$ is no longer needed to reach the WMAP-measured relic abundance. In panel (b) we show the corresponding bino/higgsino/wino content of the $\tilde{Z}_1$ versus $\tan\beta$. It is seen that over the bulk of the range of $\tan\beta$, $\tilde{Z}_1$ remains mixed dark matter, and so the qualitative features of our LM3DM scenario are relatively invariant unless $\tan\beta$ is taken near its extreme endpoints.

Prior to discussing whether Tevatron experiments can probe supersymmetry in this region of parameter space we need to study the decay patterns of the gluino and of its daughter sparticles. For reasons detailed in Ref. [13], the radiative decays $\tilde{g} \to g\tilde{Z}_i$ dominate for the gluino masses of interest at the Tevatron. In the upper panels of Fig. 4, we show the branching ratio for these various radiative decays of the gluino for $M_3 > 0$ (left panel) and $M_3 < 0$ (right panel), together with that for the sum of all its three-body decays (labeled 3), versus $m_{1/2}$. We adopt here the same parameter set as in Fig. 2. As in the preceding figures, we set M_3 so that $\Omega_{\tilde{Z}_1}h^2 = 0.11$, the WMAP central value for the CDM abundance [1]. We see that—depending on the sign of M_3—gluinos lighter than ~420–475 GeV dominantly decay radiatively. For small to medium values of

[4]In this case, the gluino lifetime becomes relatively large, and the gluino hadronizes before it can decay. We warn the reader that hadronization effects may significantly modify the relic density calculated here using the $\tilde{g}\tilde{Z}_1 \to q\bar{q}$ annihilation rate.

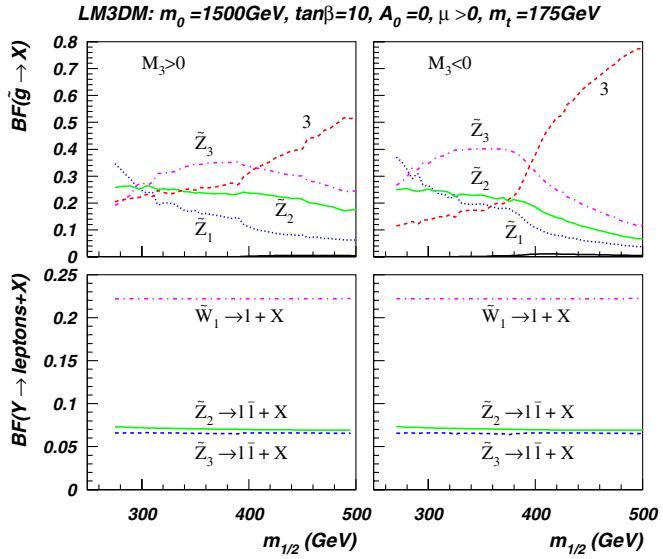

FIG. 4 (color online). The curves (labeled $\tilde{Z}_i$) in the upper panels show the branching fractions for the radiative decays $\tilde{g} \to \tilde{Z}_i g$ of the gluino versus $m_{1/2}$ for LM3DM model where $M_3(M_{\rm GUT})$ has been adjusted at every point to attain mixed higgsino dark matter with $\Omega_{\tilde{Z}_1} h^2 = 0.11$, while the curve labeled 3 denotes the corresponding branching fraction for the sum of all three-body decays of the gluino. The (barely visible) unlabeled lowest curves in the upper panels indicate $B(\tilde{g} \to \tilde{Z}_4 g)$ which is find to lie always below the percent level. The lower panels show the total leptonic branching fractions for the decays, $\tilde{Z}_2 \to \ell\bar{\ell} + X$, $\tilde{Z}_3 \to \ell\bar{\ell} + X$ and $\tilde{W}_1 \to \ell + X$, adding in all possible decay chains for the particular lepton topology. The left (right) panels are for $M_3 > 0$ ($M_3 < 0$). Everywhere, we fix $m_0 = 1500$ GeV, $A_0 = 0$, $\tan\beta = 10$ and $m_t = 175$.

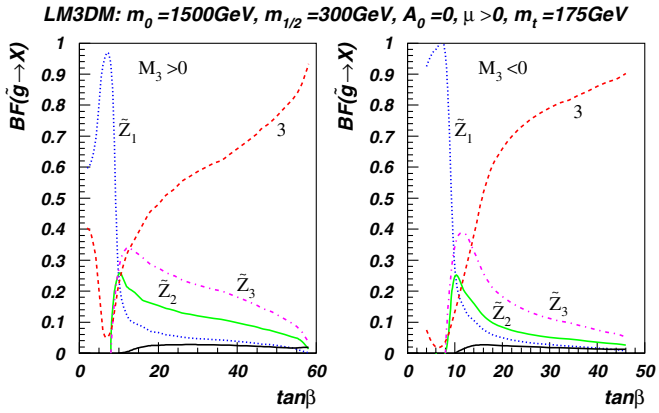

FIG. 5 (color online). Plot of gluino branching fractions to three-body modes (red-dashed curves), and various radiative decays $\tilde{g} \to g\tilde{Z}_i$, for $i = 1$–4 versus $\tan\beta$ for (a) $M_3 > 0$ and (b) $M_3 < 0$.

$\tan\beta$, where bottom quark Yukawa couplings can be neglected, the partial width for the various radiative decays is mainly governed by the $\tilde{H}_u$ content of the neutralino [13,19], and accounts for the ordering of the branching fractions for these decays. The sharp rise in the branching fraction for the three-body decays is due to the opening up of decays to the winolike $\tilde{Z}_4$ and $\tilde{W}_2$, both of which have large $SU(2)$ gauge couplings to $\tilde{q}_L$: when these modes are not phase space suppressed, they rapidly dominate the decay width. Note that unlike the tree-level decay, the radiative decay to the dominantly winolike $\tilde{Z}_4$ is dynamically suppressed because the higgsino component of the winolike state is always small. Although we have shown the results for the particular choice of $m_0 = 1.5$ TeV, we have checked that these results are qualitatively unaltered for m_0 values in the range between 1 and 2 TeV.

In the lower panels of Fig. 4 we show the cumulative leptonic branching fractions for the daughter neutralinos and charginos versus $m_{1/2}$. For $\tilde{W}_1$ and $\tilde{Z}_2$, this is simply the usual branching ratio $B(\tilde{W}_1 \to \ell\nu\tilde{Z}_1)$ and $B(\tilde{Z}_2 \to \ell\bar{\ell}\tilde{Z}_1)$, but for $\tilde{Z}_3$ the two leptons can come from either its primary decay, or from the leptonic decays of daughter neutralinos.[5] The branching fractions shown in these lower panels can be used in conjunction with those in the upper panels and the gluino production cross sections to estimate cross sections (before any cuts) for various multilepton topologies in di-jet events at the Tevatron.

For large (but not extreme) values of $\tan\beta$, the value of r_3 required to get $\Omega_{\tilde{Z}_1} h^2 = 0.11$ is larger as shown previously in Fig. 3. As a result, the gluino is relatively heavier than the various charginos and neutralinos compared to the low $\tan\beta$ case, and so gluino 3-body decays (especially decays to $\tilde{W}_2$ and $\tilde{Z}_4$) become increasingly important. The situation is illustrated in Fig. 5, where we plot gluino branching fractions versus $\tan\beta$ for the same parameters as in Fig. 4, but with $m_{1/2} = 300$ GeV and (a) $M_3 > 0$ and (b) $M_3 < 0$. While the three-body decays grow in importance with $\tan\beta$, the radiative decays remain a significant portion of the gluino branching fraction.

Finally, we note here that there exists the possibility that the cosmological dark matter may very well consist of several components, so that even lower values of r_3 (which would lead to $\Omega_{\tilde{Z}_1} h^2 < \Omega_{\rm CDM} h^2$) *are also allowed*. Within the LM3DM framework, Tevatron experiments can, and should, search for gluinos also in these lower $|r_3|$ portions of parameter space since they have not been excluded by LEP2 searches or the WMAP relic density determination. In the case of even lower $|r_3|$ values than those needed to saturate the WMAP-measured relic abundance, it is possible that the gluinos are even lighter than the values we obtain here (see, e.g. Fig. 2), and the resulting LEP2 excluded region could as well be smaller than what we show.

[5] In principle, there could be contributions from $\tilde{Z}_3 \to W^{\pm}\tilde{W}_1^{\mp}$, but these decays are kinematically inaccessible over the entire parameter space range shown in the plot.

TABLE I. Cuts used for the analysis of multi-jet + $E_T^{\rm miss}$ signatures in the LM3DM model.

cut	$2j + E_T^{\rm miss}$	$3j + E_T^{\rm miss}$	$4j + E_T^{\rm miss}$
$\Delta\phi(j_1, j_2) < 165°$	yes	yes	yes
isol. lep. veto	yes	yes	yes
n_j	≥ 2	≥ 3	≥ 4
$\lvert\eta_{j_i}\rvert < 0.8$	j_1, j_2	j_1, j_2, j_3	j_1, j_2, j_3, j_4
$80° < \Delta\phi(E_T^{\rm miss}, j_1) < 150°$	yes	yes	yes
$\Delta\phi(E_T^{\rm miss}, j_2)$	50°–150°	50°–150°	60°–150°
$E_T^{\rm miss}$	≥ 120 GeV	≥ 100 GeV	≥ 75 GeV
H_T	≥ 220 GeV	≥ 150 GeV	—

TABLE II. SM backgrounds in fb after cuts listed in Table I for the multi-jet + $E_T^{\rm miss}$ signatures in the LM3DM model.

BG	$2j + E_T^{\rm miss}$	$3j + E_T^{\rm miss}$	$4j + E_T^{\rm miss}$
$t\bar{t}(175)$	6.6 ± 0.3	12.3 ± 0.5	14.9 ± 0.6
W + jets	8.9 ± 1.4	15.5 ± 1.9	12.1 ± 1.7
Z + jets	11.0 ± 0.7	17.2 ± 0.9	9.0 ± 0.7
total	26.5	45.1	36.0

III. SEARCH IN THE JETS + $E_T^{\rm miss}$ CHANNEL

In this section, we examine whether the Fermilab Tevatron can detect gluino pair production in the LM3DM model in the multi-jet + $E_T^{\rm miss}$ mode, assuming 5 fb^{-1} of integrated luminosity that is projected to be accumulated by each experiment at the Tevatron. We generate signal and background events using Isajet 7.74, with a toy detector simulation containing hadronic calorimetry ranging out to $|\eta| < 4$, with cell size $\Delta\eta \times \Delta\phi = 0.1 \times 0.262$. We adopt hadronic smearing of $\Delta E = 0.7/\sqrt{E}$ and EM smearing of $\Delta E = 0.15/\sqrt{E}$. We adopt the Isajet GETJET jet finding algorithm, requiring jets in a cone size of $\Delta R = 0.5$ with $E_T^{\rm jet} > 15$ GeV. Jets are ordered from highest E_T (j_1) to lowest E_T. Leptons within $|\eta_\ell| < 2.5$ ($\ell = e, \mu$) are classified as isolated if $p_T(\ell) > 5$ GeV and a cone of $\Delta R = 0.4$ about the lepton direction contains $E_T < 2$ GeV. Finally, if a jet with $|\eta_j| \leq 2$ has a B-hadron with $E_T \geq 15$ GeV within $\Delta R \leq 0.5$, it is tagged as a b-jet with an efficiency of 50%.

To find optimal cuts, we generated 100K signal events for the case where $m_{1/2} = 300$ GeV, $m_0 = 1500$ GeV, $A_0 = 0$, $\tan\beta = 10$ and $\mu > 0$. For this point, $M_3 = 79.69$ GeV yields $\Omega_{\tilde{Z}_1} h^2 = 0.12$. We have also generated SM background event samples from W + jets production, Z + jets production, $t\bar{t}$ production and vector boson pair production.[6] The W or Z + jets sample uses QCD matrix elements for the primary parton emission, while subsequent emissions are generated from the parton shower.

[6]We do not estimate QCD backgrounds which, we assume, are negligible after the cuts described below [16].

We adopt a set of cuts similar to those used by the D0 collaboration in Ref. [16], but optimize the $E_T^{\rm miss}$ and H_T cut values for this framework. Our final set of cuts are listed in Table I, where we divide the signal topologies into $\geq$ 2-jets + $E_T^{\rm miss}$, $\geq$ 3-jets + $E_T^{\rm miss}$ and $\geq$ 4-jets + $E_T^{\rm miss}$, while vetoing isolated leptons. The constituent background rates from the major background sources are listed in Table II. From these rates, we can compute the signal observability level needed for a given integrated luminosity, using the following criteria: (i) the statistical significance $S/\sqrt{B} \geq 5\sigma$, (ii) $S/B \geq 25\%$, and (iii) $S \geq 10$ events.

Our results for the SUSY reach of the Tevatron within the LM3DM framework are shown in Fig. 6 versus $m_{1/2}$ for the same parameter choices as in Fig. 2. Assuming an integrated luminosity of 5 fb^{-1}, we have checked that the reach in each of the three n-jet + $E_T^{\rm miss}$ event topologies is limited by the 5σ criterion. The minimum cross section for observability of the signal is shown by the dashed horizontal line, while the signal is indicated by the solid (dashed)

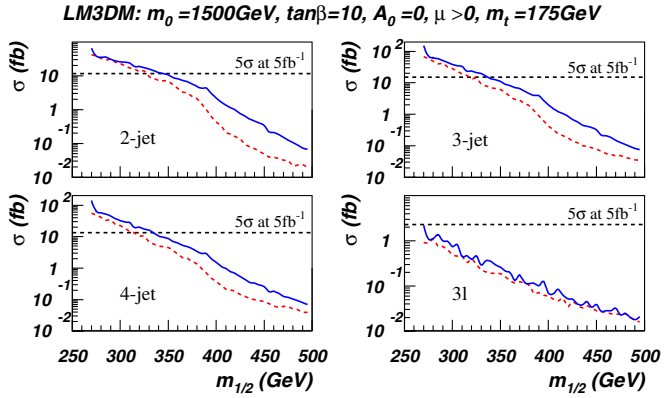

FIG. 6 (color online). The SUSY reach of the Fermilab Tevatron with 5 fb^{-1} of integrated luminosity in the multi-jet + $E_T^{\rm miss}$ channel for (a) di-jet events, (b) trijet events, (c) four jet events, and (d) trilepton events for LM3DM model where $|M_3(M_{\rm GUT})|$ has been adjusted at every point to get $\Omega_{\tilde{Z}_1} h^2 = 0.11$. We fix $A_0 = 0$, $\tan\beta = 10$, $m_t = 175$ GeV and $m_0 = 1500$ GeV, a slice representative of the LM3DM parameter space under investigation here. The solid curve is for $M_3 > 0$, while the dashed curve corresponds to $M_3 < 0$.

curve for $M_3 > 0$ ($M_3 < 0$) for (a) $\geq$ 2-jets + $E_T^{\rm miss}$ events, (b) $\geq$ 3-jets + $E_T^{\rm miss}$ events and (c) $\geq$ 4-jets + $E_T^{\rm miss}$ events. We see in each of panels (a)–(c) that the 5 fb^{-1} reach extends out to $m_{1/2} \sim 330$–340 GeV, corresponding to a reach in $m_{\tilde{g}}$ according to Fig. 2 of $\sim$320 GeV. Within the LM3DM framework, this corresponds to a reach in $m_{\tilde{W}_1} \gtrsim 170$ GeV, and thus extends well beyond that of LEP2 experiments. Although we have shown these results for $\tan\beta = 10$, we expect that the reach via these inclusive multijet plus $E_T^{\rm miss}$ searches is relatively insensitive to $\tan\beta$, except for the extremely high $\tan\beta$ values that require little reduction of $|r_3|$ because the A resonance enhancement of the LSP annihilation cross section in the early universe yields the WMAP CDM relic density.

IV. SEARCH IN THE TRILEPTON + $E_T^{\rm miss}$ CHANNEL

We have also examined the reach of the Fermilab Tevatron in the much touted inclusive trilepton channel [20] where the leptons arise from the decays of charginos and neutralinos produced via $p\bar{p} \to \tilde{W}_1\tilde{Z}_i + X$, or via cascade decays of gluinos. Since, as discussed above, the mass gap between $\tilde{W}_1/\tilde{Z}_2$ and the $\tilde{Z}_1$ LSP is not large, we expect the lepton spectra to be relatively soft. Hence, for this study, we adopt the soft lepton cuts SC2 introduced in the first paper of Ref. [21], where the background was found to be 1.05 fb. The reach in the inclusive trilepton channel is shown in Fig. 6(d) where we see that signal is always below the 5σ observability level. This is, in part, due to the fact that the kinematically favored $\tilde{W}_1\tilde{Z}_{2,3}$ production now dominantly occurs via the weak isodoublet higgsino components of the chargino and neutralino which have a smaller coupling (than the weak isotriplet coupling characteristic of the mSUGRA framework) to the Z boson. We conclude that in the case of the LM3DM model, the best search channel is the multi-jets + $E_T^{\rm miss}$ channels.

V. SEARCH IN THE JETS + OS-DILEPTON + $E_T^{\rm miss}$ CHANNEL

The relatively low value of $|\mu|$ is the characteristic feature of the LM3DM model. As a result, three (rather than two) neutralinos tend to be relatively light and mixed, whereas gaugino-higgsino mixing increases the masses of the heavier chargino and the heaviest neutralino. It is, therefore, reasonable to ask whether it is possible to identify their production via the cascade decays of gluinos at the Tevatron. We are thus led to investigate the observability of the signal in the multi-jet + opposite sign (OS) dilepton + $E_T^{\rm miss}$ channel, where the leptons have the same flavor. This channel is of special importance since it has been long known that the dilepton invariant mass spectrum from $\tilde{Z}_i \to \tilde{Z}_1 + \ell\bar{\ell}$ contains a kinematic cut-off at $m_{\tilde{Z}_i} - m_{\tilde{Z}_1}$. The mass edge(s), if visible, can serve as the starting point for reconstructing sparticle cascade decays, and for obtaining information on sparticle masses [22].

TABLE III. SM backgrounds and signal for $m_{1/2} = 300$ GeV in fb after cuts listed in text for the multi-jet + $\ell\bar{\ell}$ + $E_T^{\rm miss}$ signatures in the LM3DM model.

BG	$2j + \ell\bar{\ell} + E_T^{\rm miss}$
$t\bar{t}(175)$	11.6 ± 0.5
$Z \to \tau\bar{\tau}$ + jets	5.6 ± 0.5
WW, WZ, ZZ	7.6 ± 0.6
total	24.8
signal $m_{1/2} = 300$ GeV	21.4 ± 0.6

Toward this end, we examine the signal in the multi-jet + $\ell\bar{\ell}$ + $E_T^{\rm miss}$ channel, where $\ell = e$ or μ. We extract signal events containing two opposite-sign/same-flavor isolated leptons plus jets plus missing transverse energy, and compare the signal with SM backgrounds from $t\bar{t}$ production, $Z \to \tau\bar{\tau}$ + jets production and vector boson pair production (W^+W^-, Z^0Z^0 and $W^\pm Z^0$ production). By requiring hard missing E_T ($E_T^{\rm miss} > 75$ GeV), we reject much of the background from Z^0 production, while by requiring a veto of events with a tagged b-jet we reject much of the $t\bar{t}$ background with hardly any loss of signal. Finally, requiring at least 2 jets in the events improves the statistical significance of the signal. The surviving background rates in fb, along with signal in the LM3DM framework for $m_{1/2} = 300$ GeV and other parameters as in Fig. 2 are listed in Table III. The corresponding reach in the $\geq$ 2-jets + $\ell\bar{\ell}$ + $E_T^{\rm miss}$ channel is once again governed by the 5σ criterion, and is shown in Fig. 7 versus $m_{1/2}$, with other parameters as in Fig. 2, for 5 fb^{-1} of integrated

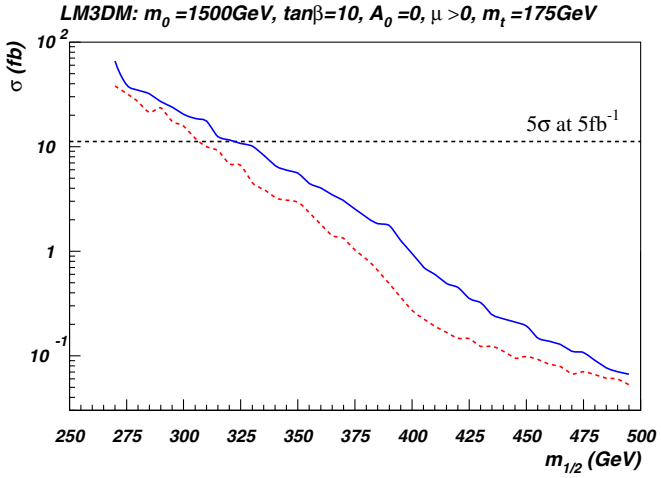

FIG. 7 (color online). The SUSY reach of the Fermilab Tevatron in the $\geq$ 2 jets + $\ell\bar{\ell}$ + $E_T^{\rm miss}$ channel for the case of $m_0 = 1500$ GeV, $A_0 = 0$, $\tan\beta = 10$ and $m_t = 175$ GeV assuming an integrated luminosity of 5 fb^{-1}. We dial $M_3(M_{\rm GUT})$ for each $m_{1/2}$ so that $\Omega_{\tilde{Z}_1}h^2 = 0.11$.

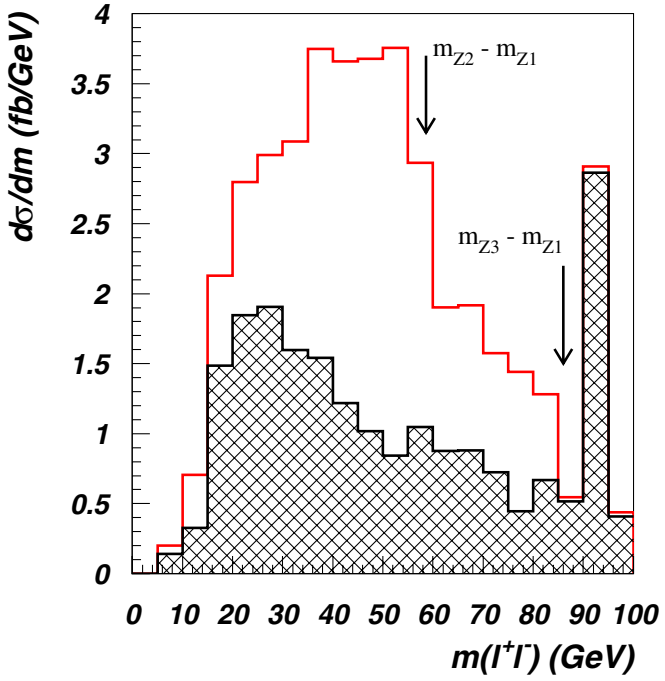

FIG. 8 (color online). The spectrum of opposite-sign/same-flavor dilepton invariant mass in background (hatched) and signal-plus-background (open histogram), for the case of $m_0 = 1500$ GeV, $m_{1/2} = 300$ GeV, $M_3 = 79.69$ GeV. We also take $A_0 = 0$, $\tan\beta = 10$ and $m_t = 175$ GeV. The arrows denote the theoretically expected positions of the corresponding mass edges.

luminosity. We see that it extends out to $m_{1/2} \sim 310$–320 GeV, i.e. slightly lower than the reach in the multi-jet + $E_T^{\rm miss}$ channels.

In order to examine the detectability of any dilepton mass edges, we show the opposite-sign/same-flavor dilepton invariant mass spectrum from the signal and background in Fig. 8, for the case of $m_{1/2} = 300$ GeV, and other parameters as in Fig. 2. The hatched distribution comes from the various background sources listed in Table III, which includes a peak at $m(\ell\bar{\ell}) = M_Z$ from Z-pair production. The signal plus background is shown by the open histogram. In this case, a distinct mass edge can be seen at $m_{\tilde{Z}_2} - m_{\tilde{Z}_1} \sim 59$ GeV. Remarkably, the mass edge from $\tilde{Z}_3 \to \tilde{Z}_1 \ell\bar{\ell}$ is also seen at $m_{\tilde{Z}_3} - m_{\tilde{Z}_1} \sim 86$ GeV. This higher mass edge will be somewhat obscured by Z-width effects, which are not included in our simulation of ZZ production. The point, however, is that the value of $m_{\tilde{Z}_3} - m_{\tilde{Z}_1}$ in our study is only fortuitously close to M_Z, and in general, it may be possible to see even the second mass edge at the Tevatron! Observation of this second mass edge would provide a strong hint for a small value of $|\mu|$.

VI. SUMMARY AND CONCLUDING REMARKS

Within the mSUGRA model, or any other supersymmetric setup with unification of the soft SUSY breaking gaugino mass parameters at the GUT scale, the lower limit $m_{\tilde{W}_1} \geq 103$ GeV from LEP2 experiments excludes gluinos with masses smaller than about 300–350 GeV, leaving little room for gluino searches at the Fermilab Tevatron. This is, however, a *model-dependent* conclusion, and, as already stressed elsewhere [18], Tevatron experiments should search for gluinos independently of the constraints from LEP2.

We provide here a specific example, the so-called low $|M_3|$ dark matter framework (LM3DM), where the universality of the GUT scale gluino mass parameter with the corresponding $SU(2)$ and hypercharge gaugino mass parameters is relaxed, while the universality of all other soft SUSY breaking parameters is retained, as in the mSUGRA setup. Except at the very upper end of the $\tan\beta$ range where A-funnel annihilation becomes operative, by adjusting the magnitude of M_3(GUT) (which can have either sign) to low values leads to SUSY spectra with relatively suppressed values of $|\mu|$, entailing, in turn, a larger LSP higgsino fraction, which can then lead to an LSP relic density in agreement with the observationally preferred central value (1) of $\Omega_{\rm CDM}h^2$ for any value of the other soft SUSY breaking parameters.

The LM3DM framework leads to characteristic differences in the sparticle spectra from the usually studied frameworks with unified gaugino masses, or with anomaly-mediated SUSY breaking. In particular, low values of $|M_3|$ imply that the $m_{\tilde{g}}/m_{\tilde{W}_1}$ ratio is significantly smaller in the LM3DM model compared to the mSUGRA case, so that experiments at the Tevatron will be able to explore regions of parameter space not already ruled out by LEP2.

The main result of the present study is the reach of the Fermilab Tevatron experiments within the LM3DM framework, shown in Fig. 6 and 7. The best reach is obtained in the inclusive multi-jet + $E_T^{\rm miss}$ channels, while the reach in the multijet plus opposite-sign dilepton channel is only slightly less effective. Assuming an integrated luminosity of 5 fb^{-1}, expected to be delivered to each experiment within the next two years of operations at the Tevatron, the reach extends up to $m_{1/2} = 350$ GeV which, for $M_3 > 0$ corresponds to $m_{\tilde{g}} \sim 325$ GeV and $m_{\tilde{W}_1} \sim 170$ GeV, significantly beyond the reach of LEP2. Combining the two experiments will yield an even higher reach.

The concomitant smallness of $|\mu|$ within this framework implies that both $\tilde{Z}_2$ and $\tilde{Z}_3$ may be accessible via gluino decays, offering another interesting opportunity to Tevatron experiments, as illustrated in Fig. 8: the invariant dilepton mass spectrum for events with ≥ 2jets + OS dileptons + $E_T^{\rm miss}$, with a veto on b-tagged jets (to reduce the background from $t\bar{t}$ production), may yield mass edges from both $\tilde{Z}_2 \to \ell\bar{\ell}\tilde{Z}_1$ and $\tilde{Z}_3 \to \ell\bar{\ell}\tilde{Z}_1$ decays. Observation of two mass edges would strongly suggest a small value of $|\mu|$.

In summary, if SUSY is realized as in the LM3DM model, a framework consistent with all constraints from particle physics and cosmology, experiments at the Tevatron will be able to probe regions of parameter space not accessible at LEP 2 before the LHC experiments turn on and collect data for physics analysis. We urge our colleagues on the CDF and D0 experiments to search for gluinos irrespective of constraints from chargino searches since these are based on the *untested* assumption of gaugino mass unification.

ACKNOWLEDGMENTS

We would like to thank A. Belyaev and J.-F. Grivaz for useful discussions. This research was supported in part by grants No. DE-FG02-97ER41022, DE-FG02-95ER40896, DE-FG03-92-ER40701, DE-FG02-ER41291, and DE-FG02-05ER41361 DE-FG02-04ER41308 from the United States Department of Energy, NASA NNG05GF69G from NASA and the Wisconsin Alumni Research Foundation.

[1] D. N. Spergel *et al.* (WMAP Collaboration), astro-ph/0603449.

[2] For recent reviews, see e.g. C. Jungman, M. Kamionkowski, and K. Griest, Phys. Rep. **267**, 195 (1996); A. Lahanas, N. Mavromatos, and D. Nanopoulos, Int. J. Mod. Phys. D **12**, 1529 (2003); M. Drees, hep-ph/0410113; K. Olive, astro-ph/0503065.

[3] A. Chamseddine, R. Arnowitt, and P. Nath, Phys. Rev. Lett. **49**, 970 (1982); R. Barbieri, S. Ferrara, and C. Savoy, Phys. Lett. B **119**, 343 (1982); N. Ohta, Prog. Theor. Phys. **70**, 542 (1983); L. J. Hall, J. Lykken, and S. Weinberg, Phys. Rev. D **27**, 2359 (1983); for reviews, see H. P. Nilles, Phys. Rep. **110**, 1 (1984); P. Nath, hep-ph/0307123.

[4] M. Drees and M. Nojiri, Phys. Rev. D **47**, 376 (1993); H. Baer and M. Brhlik, Phys. Rev. D **53**, 597 (1996); **57**, 567 (1998); H. Baer, M. Brhlik, M. Diaz, J. Ferrandis, P. Mercadante, P. Quintana, and X. Tata, Phys. Rev. D **63**, 015007 (2001); J. Ellis, T. Falk, G. Ganis, K. Olive, and M. Srednicki, Phys. Lett. B **510**, 236 (2001); L. Roszkowski, R. Ruiz de Austri, and T. Nihei, J. High Energy Phys. 08 (2001) 024; A. Djouadi, M. Drees, and J. L. Kneur, J. High Energy Phys. 08 (2001) 055; A. Lahanas and V. Spanos, Eur. Phys. J. C **23**, 185 (2002).

[5] K. Griest and D. Seckel, Phys. Rev. D **43**, 3191 (1991); J. McDonald, K. Olive, and M. Srednicki, Phys. Lett. B **283**, 80 (1992); S. Mizuta and M. Yamaguchi, Phys. Lett. B **298**, 120 (1993).

[6] J. Ellis, T. Falk, and K. Olive, Phys. Lett. B **444**, 367 (1998); J. Ellis, T. Falk, K. Olive, and M. Srednicki, Astropart. Phys. **13**, 181 (2000); M. E. Gómez, G. Lazarides, and C. Pallis, Phys. Rev. D **61**, 123512 (2000); Phys. Lett. B **487**, 313 (2000); A. Lahanas, D. V. Nanopoulos, and V. Spanos, Phys. Rev. D **62**, 023515 (2000); R. Arnowitt, B. Dutta, and Y. Santoso, Nucl. Phys. **B606**, 59 (2001); H. Baer, C. Balazs, and A. Belyaev, J. High Energy Phys. 03 (2002) 042.

[7] C. Böhm, A. Djouadi, and M. Drees, Phys. Rev. D **62**, 035012 (2000); J. R. Ellis, K. A. Olive, and Y. Santoso, Astropart. Phys. **18**, 395 (2003); J. Edsjö *et al.*, J. Cosmol. Astropart. Phys. 04 (2003) 001.

[8] K. L. Chan, U. Chattopadhyay, and P. Nath, Phys. Rev. D **58**, 096004 (1998); J. Feng, K. Matchev, and T. Moroi, Phys. Rev. Lett. **84**, 2322 (2000); Phys. Rev. D **61**, 075005 (2000); see also H. Baer, C. H. Chen, F. Paige, and X. Tata, Phys. Rev. D **52**, 2746 (1995); **53**, 6241 (1996); H. Baer, C. H. Chen, M. Drees, F. Paige, and X. Tata, Phys. Rev. D **59**, 055014 (1999); for a model-independent approach, see H. Baer, T. Krupovnickas, S. Profumo, and P. Ullio, J. High Energy Phys. 10 (2005) 020.

[9] V. Berezinsky *et al.*, Astropart. Phys. **5**, 1 (1996); P. Nath and R. Arnowitt, Phys. Rev. D **56**, 2820 (1997); A. Bottino *et al.* Phys. Rev. D **59**, 095004 (1999); **63**, 125003 (2001); J. Ellis, K. Olive, and Y. Santoso, Phys. Lett. B **539**, 107 (2002); J. Ellis, T. Falk, K. Olive, and Y. Santoso, Nucl. Phys. **B652**, 259 (2003); H. Baer, A. Mustafayev, S. Profumo, A. Belyaev, and X. Tata, Phys. Rev. D **71**, 095008 (2005); J. High Energy Phys. 07 (2005) 065; C. Lester, A. Parker, and M. J. White, hep-ph/0609298; L. Solmaz, hep-ph/0609162.

[10] A. Birkedal-Hansen and B. Nelson, Phys. Rev. D **64**, 015008 (2001); **67**, 095006 (2003); H. Baer, A. Mustafayev, E. Park, and S. Profumo, J. High Energy Phys. 07 (2005) 046.

[11] H. Baer, T. Krupovnickas, A. Mustafayev, E. Park S. Profumo, and X. Tata, J. High Energy Phys. 12 (2005) 011.

[12] Y. Mambrini and E. Nezri, hep-ph/0507263; G. Belanger, F. Boudjema, A. Cottrant, A. Pukhov, and A. Semenov, Nucl. Phys. **B706**, 411 (2005).

[13] H. Baer, A. Mustafayev, E. Park, S. Profumo, and X. Tata, J. High Energy Phys. 04 (2006) 041.

[14] S. Profumo and C. Yaguna, Phys. Rev. D **69**, 115009 (2004).

[15] B. Abbott *et al.* (D0 Collaboration), Phys. Rev. Lett. **83**, 4937 (1999); T. Affolder *et al.* (CDF Collaboration), Phys. Rev. Lett. **88**, 041801 (2002).

[16] V. M. Abazov *et al.* (D0 Collaboration), Phys. Lett. B **638**, 119 (2006).

[17] H. Baer, F. Paige, S. Protopopescu, and X. Tata, hep-ph/0312045.

[18] See e.g. H. Baer and X. Tata, *Weak Scale Supersymmetry* (Cambridge University Press, Cambridge, England, 2006).

[19] H. Baer, X. Tata, and J. Woodside, Phys. Rev. D **42**, 1568 (1990).

[20] H. Baer and X. Tata, Phys. Rev. D **47**, 2739 (1993).

[21] H. Baer, M. Drees, F. Paige, P. Quintana, and X. Tata, Phys. Rev. D **61**, 095007 (2000); V. Barger and C. Kao, Phys. Rev. D **60**, 115015 (1999); K. Matchev and D.

Pierce, Phys. Lett. B **467**, 225 (1999); For a review, see S. Abel *et al.*, hep-ph/0003154.

[22] H. Baer, K. Hagiwara, and X. Tata, Phys. Rev. D **35**, 1598 (1987); H. Baer, D. Dzialo-Karatas, and X. Tata, Phys. Rev. D **42**, 2259 (1990); H. Baer, C. Kao, and X. Tata, Phys. Rev. D **48**, 5175 (1993); H. Baer, C. H. Chen, F. Paige, and X. Tata, Phys. Rev. D **50**, 4508 (1994); I. Hinchliffe *et al.*, Phys. Rev. D **55**, 5520 (1997); **60**, 095002 (1999); H. Bachacou, I. Hinchliffe, and F. Paige, Phys. Rev. D **62**, 015009 (2000); Atlas Collaboration, Report No. LHCC 99-14/15 (unpublished).